Journal of The Electrochemical Society, **158** (5) B526-B535 (2011)
0013-4651/2011/158(5)/B526/10/$28.00 © The Electrochemical Society

Evaluation of SOFC Interconnects Made of Ferritic Steels with Nano-Structured Oxi-Ceramic Protective Coatings Deposited by the LAFAD Process

V. I. Gorokhovsky,[a,*,z] P. E. Gannon,[b,*] J. Wallace,[c] D. VanVorous,[c] C. Bowman,[c] M. C. Deibert,[b] and R. J. Smith[b]

[a]*University of Texas at San Antonio, San Antonio, Texas 78249, USA*
[b]*Montana State University, Bozeman, Montana 59717, USA*
[c]*Arcomac Surface Engineering, LLC, Bozeman, Montana 59715, USA*

When Solid Oxide Fuel Cells (SOFCs) are operated in the temperature range from 750 to 800°C, it becomes possible to use inexpensive ferritic steels as interconnects (ICs). Due to the demanding SOFC-IC operating environment, protective coatings are gaining attention as a way to increase long-term stability. In this study, the large area filtered arc deposition (LAFAD) process was used to deposit nano-structured coatings from the (Co,Mn)TiCrAlY(O,N) system. Both nano-laminated as well as nano-composite coating architectures were studied and compared. Coatings were deposited on ferritic steel with the aid of an ultra-thin, adhesion-promoting bond-coat, and were subsequently annealed in air for various time intervals. Surface oxidation was investigated using RBS, SEM, and EDS analyses. Cr-volatilization was evaluated using a modified transpiration apparatus and Area Specific Resistance (ASR) was studied as a function of time using a four-point technique. Significant improvement in oxidation resistance, Cr volatility, and ASR were observed in the coated samples. In addition, a set of sample IC plates were subjected to LAFAD coatings and tested in a SOFC stack. Transport mechanisms for various oxidizing species and coating diffusion barrier properties are discussed, as are the trades-offs between ionic diffusion and electronic conductivity.
[DOI: 10.1149/1.3559156]

Manuscript submitted August 2, 2010; revised manuscript received January 21, 2011. Published March 21, 2011.

Background

Planar Solid Oxide Fuel Cells (SOFCs) are increasingly promising candidates for future energy conversion due to their inherently high efficiencies and decreased environmentally sensitive emissions.[1] Typical anode-supported planar SOFC design and operation are described elsewhere.[1,2] During operation, the planar SOFC interconnect (IC) component will be exposed to both wet reducing atmospheres and also to oxidizing atmospheres at temperatures up to ~800°C. The IC/electrode and IC/seal interfaces must exhibit chemical, thermal-mechanical and electrical stability throughout the desired SOFC stationary device lifetime of greater than 40,000 h, while enduring a large number of thermal cycles.[3]

High-temperature metallic alloys have received attention for use as intermediate-temperature (600–800°C) SOFC-ICs due to their higher relative toughness and formability and much lower costs compared to commonly-used ceramic alternatives. Of particular interest are high Cr-content, ferritic stainless steels, which exhibit compatible thermal expansion coefficients with other SOFC components, but form electrically resistive thermally grown oxide (TGO) scales when exposed to the complex SOFC operating gasses. TGO scales can introduce adverse chemical and thermal-mechanical incompatibilities with adjoining SOFC components through deleterious species volatilization, interdiffusion and thermal-mechanical stresses. A thorough investigation of several heat-resistant alloys concluded that for improved oxidation resistance and electrical conductivity either new alloys need to be developed, or surface engineering of existing alloys is required.[4] Among the candidates in the former category is Crofer 22 APU, a ferritic stainless steel (FSS) containing 20–24% Cr, with engineered additions of Mn, Ti and La (developed by the Quadakkers group at Forschungszentrum Jülich and available from ThyssenKrupp VDM).[5] This special high-temperature stainless steel is characterized by the formation of a stable and electrically conductive Cr-Mn oxide surface layer during SOFC cathode gas-phase exposure. However, continued TGO scale growth (dominated by an underlying Cr_2O_3 layer) during extended exposures may create increased electrical resistance and other SOFC incompatibilities.[6] High chromium ferritic stainless steels also create another problem for SOFC application: Cr poisoning of the cathode.[7,8]

To mitigate the TGO growth and eliminate Cr poisoning, different conductive oxide and nitride surface coatings (deposited by a variety of techniques) have been evaluated.[2,9–18] One of the more promising compositions is $(Co, Mn)_3O_4$ spinel (with Co:Mn – 1:1), which can provide the necessary low area surface resistance (ASR) required for this application. This coating can be deposited both by aqueous processes (e.g., sol-gel, electroplating) and by vacuum physical vapor deposition (PVD) processes such as magnetron sputtering (MS), electron beam physical vapor deposition (EBPVD) and cathodic arc deposition (CAD).[16] Conventional metal vapor sources can provide high deposition rates, but the low energy of the metal vapor atoms results in low density, poor adhesion, and poor structure and morphology of the coatings. It is well established that assistance of the coating deposition process with bombardment by energetic particles can dramatically improve coatings by densification of the depositing materials, reducing the grain size and improving coating adhesion. In these processes, the surface layer is subjected to a high rate of bombardment by energetic ions, which affects the mobility of the depositing metal vapor atoms and in many cases creates metastable structures with unique functional properties.[7,19–21] This approach is especially productive in the deposition of nano-structured and/or nanocomposite coatings with ultra-fine or glass-like amorphous structure. However, conventional EBPVD and MS processes produce metal vapor flow with very low ionization rate, usually less than 1%.

The direct cathodic arc deposition (DCAD) process produces highly ionized vapor plasma, but suffers from the large quantity of macroparticles or droplets emitted from the evaporation target surface along with atomic neutral vapor particles and ions.[7,19] The filtered cathodic arc deposition (FCAD) process, on the other hand, is able to eliminate unwanted macroparticles, droplets and most of the neutrals from the metal plasma stream generated by cathodic vacuum arc process and can produce nearly 100% ionized, atomically-clean, metal vapor plasma with a relatively high electron temperature of 3–5 eV. The metal ion flow produced by the FCAD process consists of multi-charged ions with large kinetic energy ranging from 40 to 200 eV.[7,19] Large Area Filtered Arc Deposition (LAFAD) technology provides a highly productive, robust, industry-friendly process which combines the high productivity rate of conventional DCAD and magnetron sputtering sources, with the capability of generating a nearly 100% ionized metal-gaseous vapor plasma having large kinetic energy and no macroparticles, droplets, multi-atom clusters or other contaminants.[7,22,23] Since the LAFAD plasma source operating pressure regimes overlap with most other conventional vacuum

---

[*] Electrochemical Society Active Member.
[z] E-mail: vigase@aol.com

Table I. First iteration of LAFAD nanolaminated oxi-ceramic protective coatings for SOFC IC application.

Coating designation	LAFAD targets	Approximate composition (atom %) all <1%Y; balance O
TiCrAlYO	TiCrAlY/CrA1Y	23Al–14Cr–3Ti
CoCrAlYO	CoCrAlY/CrA1Y	18Al–14Cr–12Co
TiMnCoCrAlYO	CoMn/TiCrAlY	12Mn–10Al–9Cr–3Ti–<1Co

vapor deposition technologies such as magnetron sputtering, EBPVD, thermal evaporation, plasma-assisted chemical vapor deposition (PACVD), it can be used in hybrid processes combining its high deposition and high ionization rates in conjunction with conventional PVD and low pressure PACVD processes as was demonstrated in.[7,22,24,25] The present research of high temperature thermal-chemical and mechanical stability and performance characteristics of the ferritic interconnect plates with LAFAD coatings is aimed toward understanding the influence of coating characteristics (thickness, structure, phase and chemical composition) on the long-term thermal-mechanical and chemical stability of the interconnect/cathode interface during SOFC-exposure.

Experimental

Coating design and LAFAD process parameters.— In this work nanostructured coatings of the CoMnTiCrAlY(O,N) elemental system were tested and evaluated to select the optimal composition as oxidation resistant, Cr retaining, high temperature, electrically conductive coatings for metallic alloys of SOFC interconnects. All coatings were deposited using the LAFAD hybrid deposition system; detailed description of this highly versatile system can be found elsewhere.[7,22,23,26] The typical LAFAD plasma vapor deposition trials reported in this work were performed when the substrates were mounted on pedestals distributed about the outer rim of a rotating turntable in the LAFAD batch coating system processing chamber with single rotation (SR) at 12 RPM. In SR mode, the substrates rotate around the axis of the turntable with their front surface facing the chamber walls. The coating process consists of pre-heating to 350°C, twenty minutes of ion cleaning, and two minutes of high voltage metal ion etching at –1000 V, followed by coating deposition steps in a pressure range from 4 to 8×10^{-2} Pa. Note that during deposition of nearly dielectric oxi-ceramic and oxi-nitride coatings, a 13.56 MHz RF generator was used as a substrate bias power supply, while for deposition of conductive coatings, an MDX-II (Advanced Energy) power supply, coupled with the Sparc-le V accessory, was used as a DC bias power supply. The substrate bias during deposition of most of the conductive coatings reported in this work was –40 V, while during deposition of oxiceramic and oxinitride coatings the autopolarization bias potential ranged from –40 to –100 V.

For deposition of the TiCrAlY(O,N) monolithic nanocomposite coatings, two identical Ti20Cr30Al48Y2 targets, made by a hot press technique were installed in the primary DCAD sources of the LAFAD vapor plasma source (target composition is shown in atomic percent). For deposition of more complex coatings having either cobalt or cobalt and manganese added to the TiCrAlY(O,N) matrix, one of the primary DCAD sources of the LAFAD plasma source was provided with either a Co50Mn50 target or with a target made of the so-called 'Cocrally' Co28Cr30Al29Y2 alloy. For deposition of nanocomposite monolithic coatings, the divided anode baffle of the LAFAD source was removed to allow the two opposite plasma flows generated by the primary DCAD source to be freely mixed in the filter tunnel to deposit a nanocomposite multielemental coating. Substrate temperature during deposition of the (Co,Mn)TiCrAlY(O,N) coating layer was about 500°C. Substrates were first cleaned in an Argon plasma at 8×10^{-2} Pa for twenty minutes, followed by two minutes of high voltage (–1000 V bias) Co–Cr–Al metal ion bombardment in Ar at 2×10^{-2} Pa. Cr–Co and Al ions were then deposited in a 60% O_2:40% N_2 reactive gas atmosphere with 3% Ar addition at $\sim 4 \times 10^{-2}$ Pa. In addition, the preliminary experiments were conducted with different O/N ratios to study the oxidation kinetics of these CrAlON based coatings. For deposition of nanolaminated coatings, the anode-baffle was re-installed within the plasma guide chamber of the LAFAD plasma source. The anode baffle allows the two plasma flows generated by the opposite primary DCAD sources of the dual arc unidirectional LAFAD metal vapor plasma source to be separated. For example, in the case, when both primary DCAD sources are equipped with targets having different composition and turntable rotation is engaged, the substrates were successively exposed to Cr/Co then Al ions, in a mixed O_2/N_2 reactive gas atmosphere, resulting in nanometer size

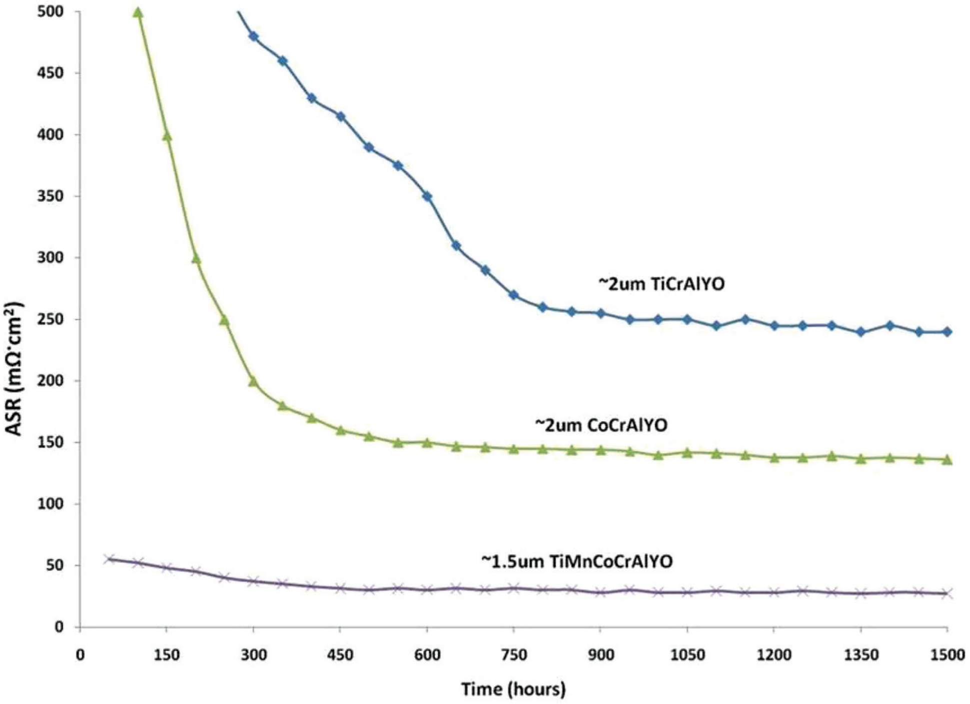

Figure 1. (Color online) ASR measurements vs time for three nanolaminated coatings presented in Table I. Porous LSM electrode contact in 800°C air.

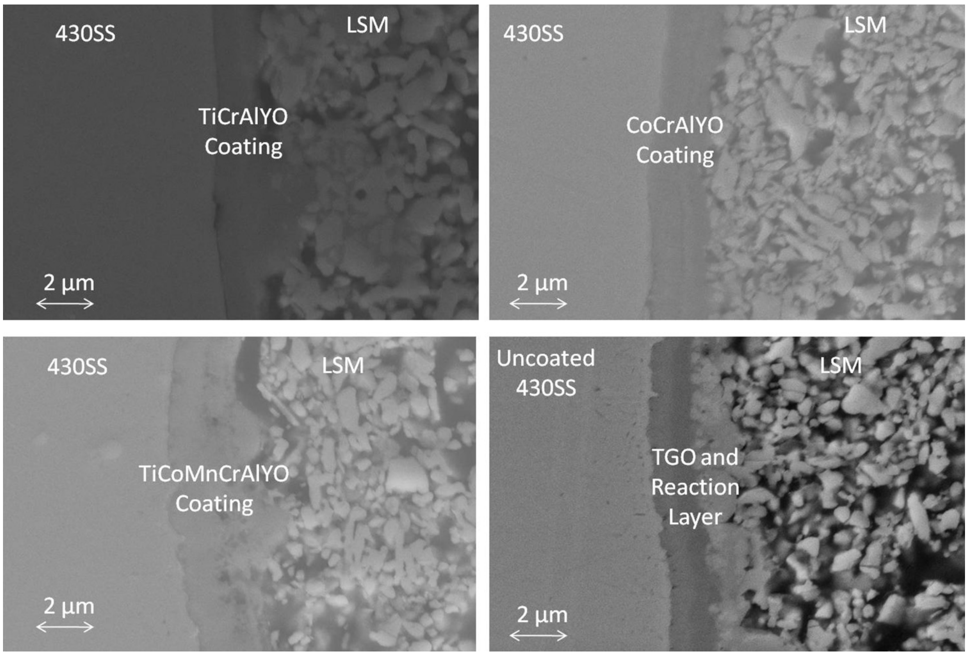

Figure 2. Cross sectional SEM images of LAFAD coated and uncoated 430SS subsequent to 1,500 h ASR testing in contact with LSM at 800°C in air. Beginning in the upper-left corner and moving clockwise are: the TiCrAlYO coating; the CoCrAlYO coating; the uncoated 430 SS; and, the CoMnTiCrAlYO coating.

bi-layers of CrCoO/N/AlO/N. Thickness of the individual bi-layers as well as total coating thickness may be controlled by the rotation speed of the carousel and deposition time.

Coating characterization.— The LAFAD coatings were characterized by their basic mechanical properties: hardness, adhesion and cohesion toughness, and surface profile. Coating thickness was determined by the CALO wear scar spherical abrasion technique and optical micrometry to an accuracy of ±0.1 μm. Coating thicknesses were also measured by metallographic cross-section followed by SEM imaging analysis. Adhesion evaluation was performed by the Rockwell-C 145 kgf indentation test according to.[28] Based on this classification, radial cracks surrounding the indentation indicate good coating adhesion. Radial cracks with localized delamination indicate fair adhesion, and concentric cracks around the indentation with large area delamination indicate poor coating adhesion. In addition, SEM imaging of the micro-cross section of the Rockwell indentation was also used to assess the fracture resistance of the coatings. Coating hardness and Young's modulus were measured by an MTS-XP nanoindenter with a CSM module and a Berkovich tip. Average coating RMS and Rz roughness were measured per ASTM B46.1 with a Veeco Dektak 8 contact profilometer. Parameters for RMS measurement were as follows; 5 μm radius stylus, 1750 μm scan length, 250 μm cutoff filter (waviness filter) and 1 data point/micrometer. Five RMS scans were made per sample and a minimum of six samples were scanned resulting in a 30-point RMS average per unique coating type reported. The internal stress in the coatings was determined by the radius of curvature technique which compares the curvatures of bare silicon substrates vs coated silicon substrates. The stress was then calculated by the Stoney formulae. Coating compositions were analyzed by EDS, RBS, XPS and Auger techniques.

Oxidation of the sample coupons in air was carried out using a standard furnace operated with no control of humidity or air circulation. Measurements of Area Specific Resistance (ASR) were made

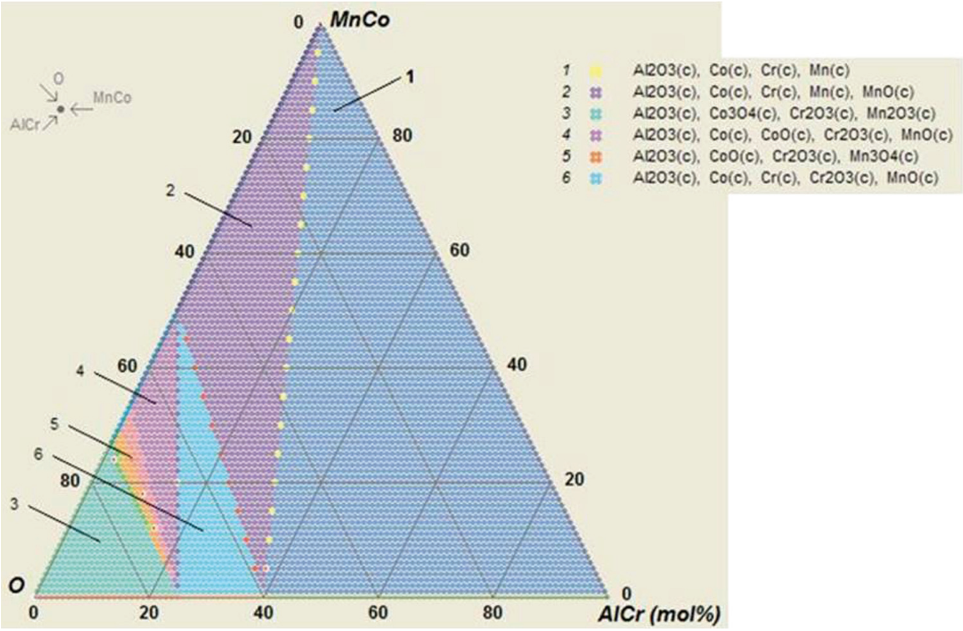

Figure 3. (Color online) Ternary phase diagram of (Co,Mn)(Cr,Al)O oxi-ceramic system calculated using TERRA computational thermodynamics codes in approximation of immiscible phases. T = 1073 K, p = 0.1 Mpa; index c relates to condense phases.

Table II. Second iteration nanocomposite CoMnTiCrAlY(O,N) coatings. All coatings except Item #5 have a 100 nm thick TiCrAlO adhesive interlayer interfacing the substrate.

Item#	Primary cathode target composition (total arc current per target I_{arc}, A) Left/Right	Coating designation (atomic composition)	Average and (Max) deposition rate over 500 dia × 15 cm tall deposition zone, micrometer per hour	Average and (Max) thickness over 500 dia × 15 cm tall deposition zone, micrometer	RMS roughness pre-/post-deposition, micrometer[a]	Hardness/ elastic modulus, GPa	Notes
1	Ti20Cr30Al48Y2(120)/ Ti20Cr30Al48Y2(120)	Ti11Cr26Al15Y1N42(O4)-SL[b]	(6.96)	3.47 (2.99)	–	48/591	–
2	Ti20Cr30Al48Y2(140)/ Ti20Cr30Al48Y2(140)	Ti5Cr19Al21Y1O54-SL	5.25 (6.3)	(12.6)	0.02/0.07	30/290	Fig. 4 top.
3	Ti20Cr30Al48Y2(140)/ CoCrAlY(120)	Co9Ti4Cr18Al18Y1O49-SL	3.06 (3.8)	(4.24)	0.02/0.05	27/255	Fig. 5 top.
4	Ti20Cr30Al48Y2(100)/ Co50Mn50(120)	Co6Mn6Ti3Cr11Al18Y2O54-SL	3.94 (4.61)	(8.68)	0.02	21/243	Fig. 7 bottom
5	Ti20Cr30Al48Y2(100)/ Co50Mn50(120)	Co10Mn6Ti4Cr14Al14Y2O50-SL	–	(3.00)	0.02	21/243	This coating did not have an insulating TiCrAlYO bond sublayer.
6	Ti20Cr30Al48Y2(140)/ Ti20Cr30Al48Y2(140)	Ti6Cr17Al23Y1O48N6-SL	4.79 (4.13)	(7.99)	0.02/0.06	27/265	Fig. 4 bottom.

[a] Roughness was measured by a Dektak 8 precision profilometer on coatings deposited on polished 440A SS.

[b] Te concentrations of respective elements by AES and EDS analysis are shown in at% after each element in coating designation formulae.

using standard procedures with Pt, Ag or SOFC cathode paste electrodes on pre-oxidized samples as a function of time and temperature for coated and uncoated SS coupons.[24] Samples exposed to high temperature ASR test environment for a various times were subsequently cross-sectioned for microscopic analysis followed by epoxy mounting, sectioning and polishing. SEM/EDS analysis was performed using a Zeiss 55 VP Supra or Jeol SEM model S4700.

Ion beam analysis of the coated samples was performed using the 3 MV tandem accelerator at the Environmental Molecular Sciences Laboratory (EMSL) at Pacific Northwest National Laboratory (PNNL) in Richland, WA, and the 2 MV van de Graaff accelerator at Montana State University. The latter was used for beams of He$^+$ and H$^+$ up to 2 MeV, while the former provided higher energy He$^+$ beams to analyze thicker coatings, and D$^+$ beams for nuclear reaction analysis of the O and N concentrations, using the ^{14}N(d,p)^{15}N and ^{16}O(d,p)^{17}O reactions. Spectra were typically collected after total oxidation periods of 1, 4, 9, 16 and 25 h at 800°C in lab air with no control of humidity. The samples were removed from the oven for ion beam analysis, and were thus subjected to thermal cycling at a rate of $\sim$25°C/min that might have adversely affected the coatings. Composition profiles were determined by comparing SIMNRA computer simulations of the spectra with the original data.[26,29,30]

Chromium volatility from coated and uncoated 441 stainless steel (SS441) samples was investigated using the transpiration apparatus described by Collins et al.[31]

Results and Discussion

Characterization of nanolaminated LAFAD coatings.— At the first iteration stage, a set of nanolaminated coatings were deposited using one unidirectional LAFAD source. These coatings have demonstrated nearly the same or even better structural and morphological properties than previously reported two-segment coatings of similar compositions deposited by LAFAD+EBPVD hybrid process and LAFAD superlattice CrAlN coatings.[2,7,24,26] The best performance was observed with LAFAD nanolaminated (amorphous/nanocrystalline) coatings ($\sim$2 μm thick) containing Co, Mn, Al, Ti, Cr and Y oxides (and solid solutions thereof) deposited on 430 SS. These coatings appear to combine the proven benefits of (Co, Mn)-oxide spinels, e.g., low ASR, decreased thermally-grown oxide growth rates, cathode compatibility, with the known diffusion-barrier properties of Al and Cr oxides. Three of these coatings are presented in Table I.

Figure 1 displays the ASR values of these coatings in contact with porous La$_{0.8}$Sr$_{0.2}$MnO$_3$ (LSM) – a common SOFC cathode – at 800°C in air. ASR values for each coating decrease from initial values. This phenomenon has been attributed to coating evolution, e.g., recrystallization, and outward transport of Mn from the steel through the coating, and was discussed in previous reports and in published literature. The lowest ASR values are realized with the (Co,Mn)-containing coating, e.g., "CoMnTiCrAlYO", which also demonstrates excellent thermal stability.[32]

Figure 2 presents cross-sectional SEM images of coated and uncoated 430 SS coupons after 1,500 h of ASR testing with LSM contact. All of the coatings have retained their as-deposited $\sim$2 μm thickness through the 1500 h ASR test, with some exhibiting compositional stratification (Mn-rich surface crystallites above amorphous alumina base-layer). During the same exposure, the uncoated 430 SS (lower right corner) has evolved a TGO layer of >10 μm thickness in some regions, with other regions of reaction with LSM (presumably forming LaCrO$_3$).

It was found that some coatings retained their as-deposited amorphous structure after more than 1,500 h exposure in 800°C air, which demonstrates the high thermal-chemical stability of this coating design during high temperature exposure.[32]

Characterization of nanocomposite monolithic LAFAD coatings.— A second iteration of LAFAD process runs were performed by using targets having either identical or different multielemental composition. In these processes, the dividing baffle was removed allowing a free mixing of two opposite vapor plasma flows in the plasma guide chamber. The fully mixed multi-elemental plasma was then deposited on substrates rotating on the substrate turntable of the FAPSID processing chamber to form various nanocomposite coatings of the (Co,Mn)TiCrAlY(O,N) elemental system. The phase composition of the (Co,Mn)TiCrAlY(O,N) nanocomposite

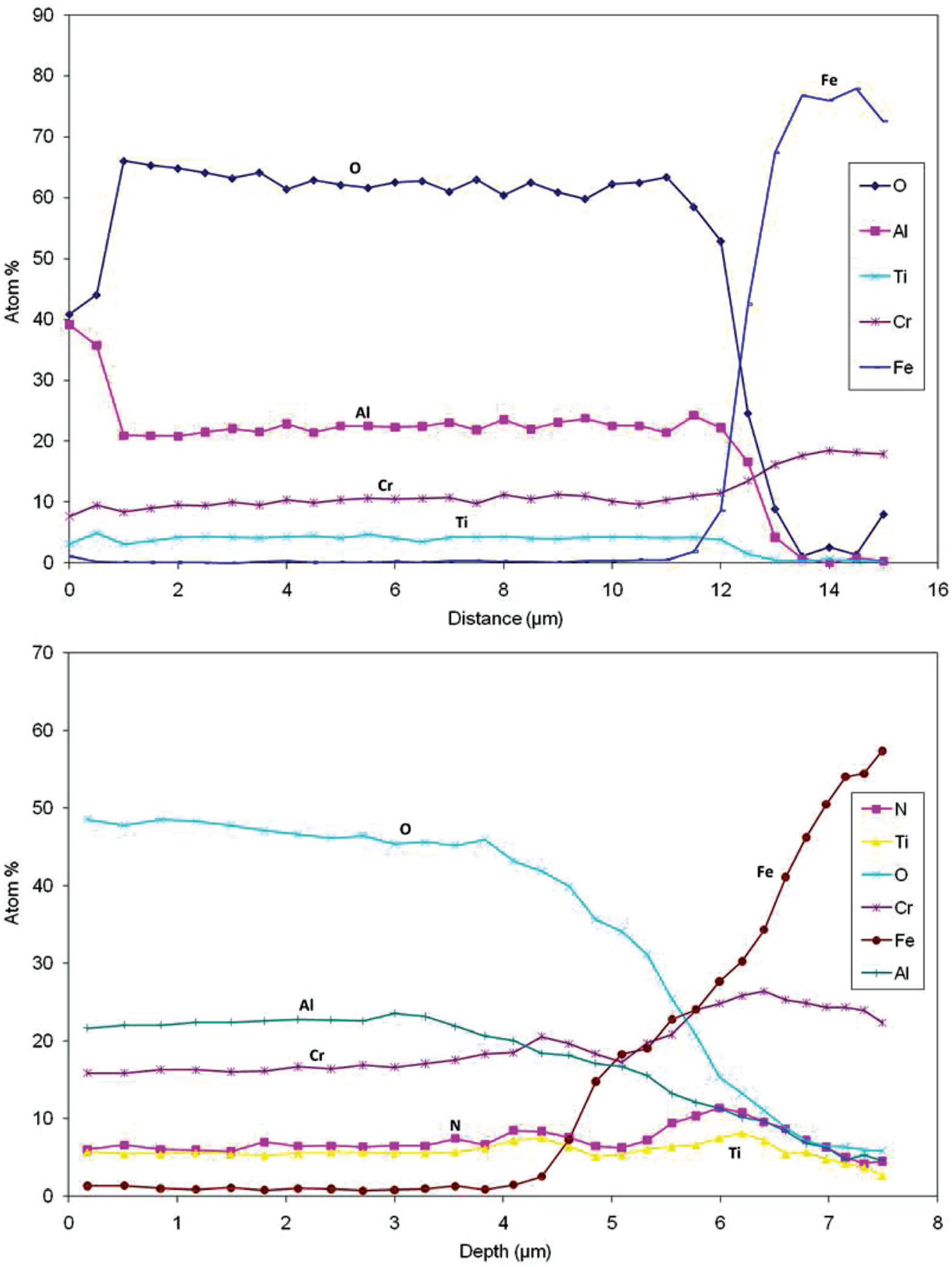

Figure 4. (Color online) An EDS line scan of TiCrAlYO (top) and TiCrAlYON (bottom) monolithic nanocomposite coatings deposited by one unidirectional LAFAD source with primary DCAD sources equipped with the same Ti20Cr30Al40Y2 targets (Table II, items # 2,6) during a 2 h coating deposition run on substrates installed on the rotating turntable of the industrial batch coating system.

coatings can be estimated using a simplified ternary phase diagram shown in Fig. 3. This diagram was prepared using TERRA computational thermodynamics software[33] with a data base of the thermodynamic properties taken from.[34,35] This calculation was carried out using the simplest model considering only immiscible phases without solid solutions.[36] It can be seen that in the area of the diagram adjacent to the oxygen corner with high concentrations of Co and Mn vs CrAl components, all phases exist in their stoichiometric oxide states. In this study, we investigated various combinations of these stoichiometric oxides as well as solid solutions thereof.

The composition of the coatings deposited in these second iteration runs, as well as their respective deposition rates and mechanical properties, are presented in Table II.

Figure 4 (top) shows the EDS line scan of a 12 μm thick TiCrAlYO monolayer coating deposited by the unidirectional LAFAD plasma source with two primary sources equipped with Ti20Cr30Al40Y2 targets on substrates installed on the rotating turntable of the batch coating system (Table II, item #2). The results of composition analysis of the nanocomposite coatings deposited by the LAFAD process using either identical or different primary cathode targets are also presented in Table II. Figure 4 (bottom) presents an EDS elemental line scan of a 6 μm thick TiCrAlYON coating (Table II, item #6). It can be seen that the metal fraction compositions of the TiCrAlY(O,N) coatings deposited by using the same primary targets closely resemble the respective target composition. The maximum deposition rate of the TiCrAlYO coating, deposited without vertical rastering of the plasma flows on substrates located near the center line of the LAFAD source exit window, exceeded 6 μm/h, while the average rate inside of the 0.15 m deposition area around the center line of the LAFAD source exit was 5.25 μm/h. Similar deposition rates have been achieved for a variety of oxiceramic, oxinitride and nitride coatings based on the TiCrAlY system with the addition of Co and Mn, as shown in Table II.

The EDS line scan in Fig. 5 (top) shows the elemental distribution across a 3 μm thick CoMnTiCrAlYO coating deposited during a forty minute deposition time by the LAFAD plasma source with

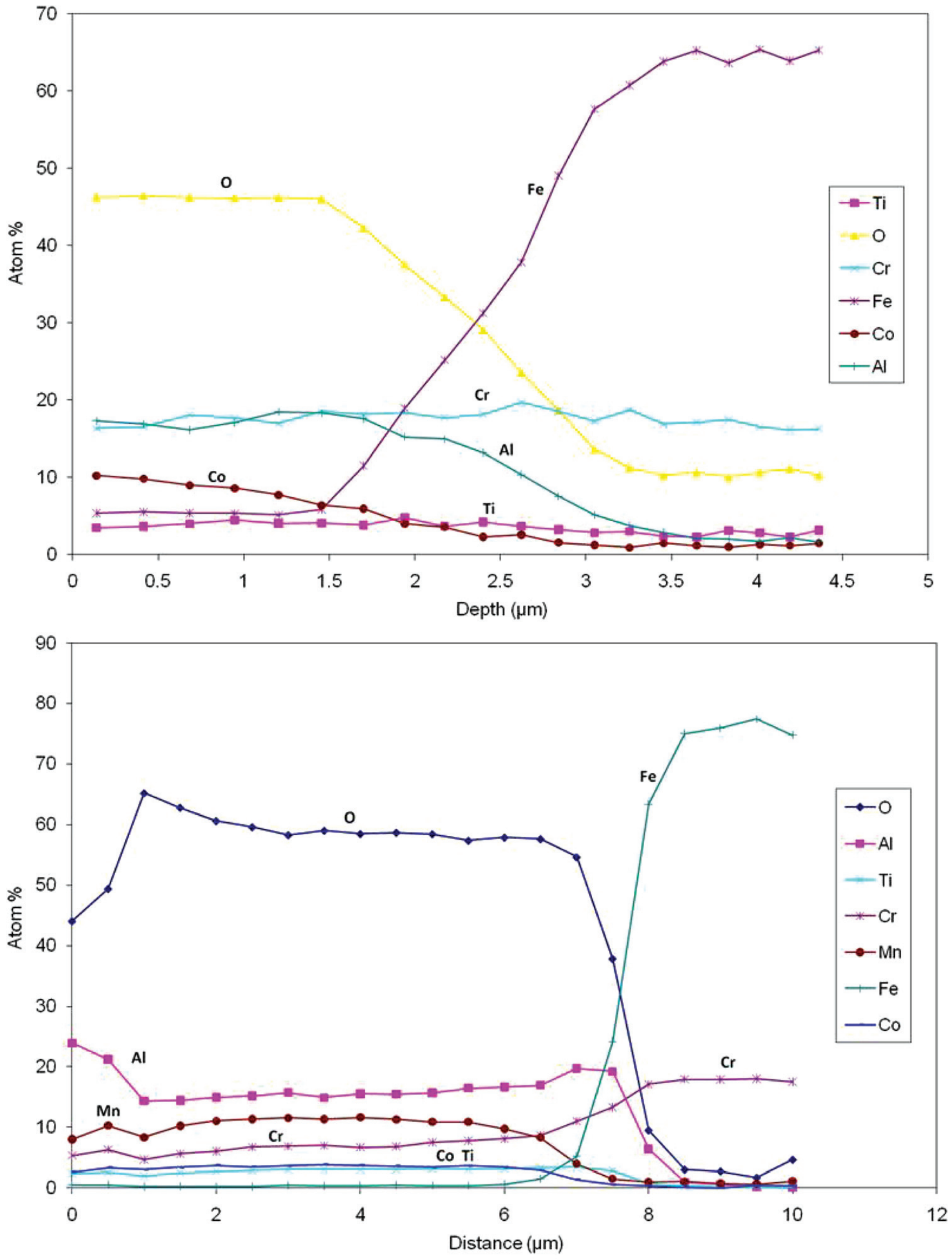

Figure 5. (Color online) An EDS line scan of CoTiCrAlYO (top) and CoMnTiCrAlYO (bottom) single layer coatings (Table II, Items 3,4 respectively) deposited by one LAFAD source with primary DCAD source #1 equipped with a Ti20Cr30Al40Y2 target and DCAD source #2 equipped with a CoCrAlY target for deposition of the coating #3 and Co50Mn50 target for deposition of the coating #4 on substrates installed on the rotating turntable of the industrial batch coating system.

two different primary arc targets: a Ti20Cr30Al48Y2 target installed on one primary source and a CoCrAlY target installed on the other primary arc source (Table II, item #3). Figure 5 (bottom) presents the elemental distribution in an 8 μm CoMnTiCrAlYO LAFAD coating (Table II, item #4) using TiCrAlY and Co50Mn50 primary arc targets. It can be seen that the LAFAD process allows effective mixing of the two filtered arc plasma flows generated by primary targets with different multi-elemental compositions to achieve deposition of complex multi-elemental nanocomposite coatings at high deposition rates.

Figure 6 presents a summary of Cr volatility results from uncoated and LAFAD TiCrAlYO coated FSS. The graph (Fig. 6a) displays the cumulative amount of Cr collected during the test. The uncoated FSS continues to volatilize Cr throughout the test, while the coated specimen demonstrates negligible Cr volatility after the first 24 h. This coating contains approximately twelve atomic percent Cr; however, the Cr is apparently sequestered in a solid solution with complex Al-containing oxides, which agrees well with thermochemical modeling.[32] Figure 6b depicts the amount of Cr condensed on Si substrates for coated and uncoated SS441 samples as measured by RBS over 24 h of collection in humid air at 800°C. The one-side coated sample volatilized less than half (approximately 38%) of the Cr that was released from the uncoated sample. The observed reduction in volatility could be expected, since the coating covered approximately 60% of the sample's surface. The two-side coated sample further reduced Cr volatility by about 54% compared with the one-side coated sample. However, the two-side coated sample exhibited significant spallation of the coating during the heating process. Thus the performance of this coating was not optimal, yet did offer a significant decrease in Cr volatility as compared with the uncoated sample.

From Table II it can be seen that the hardness of oxiceramic and oxinitride coatings of the (Co,Mn)TiCrAlY(O,N) elemental system ranges from 20 to 30 GPa, with superhard properties demonstrated by the single-layer TiCrAlYN nitride coating. It was also found that the stress level in these coatings increases with increasing nitrogen

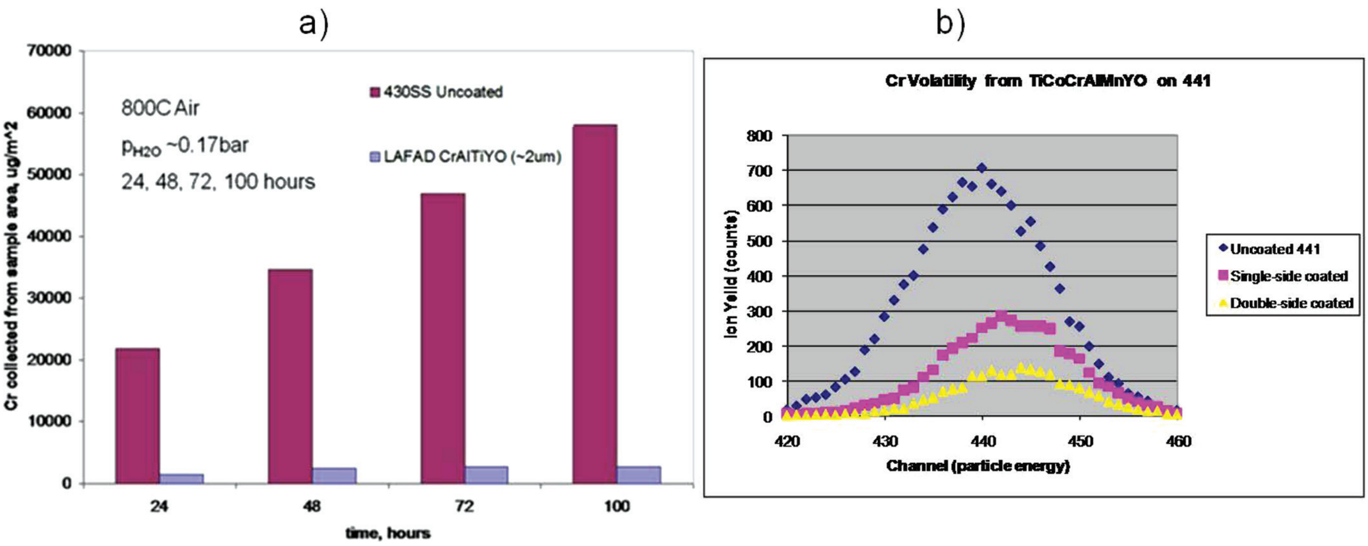

Figure 6. (Color online) Cumulative chromium volatilization rates: (a) Cr volatilized from uncoated and ~2 μm TiCrAlYO LAFAD coated FSS 430; (b) RBS spectra depicting Cr peaks for uncoated SS441 and TiCoCrAlMnYO coated SS441 over 24 h of collection in humid air at 800°C.

content, correlating with the hardness. The mechanical properties of the coatings were analyzed once again after 1500 h of oxidation at 800°C in the ASR test environment. Hardness values for coatings with Co, Mn and N decreased following these exposures, which is attributed recrystallization and N replacement with O. Hardness values for TiCrAlYO coatings did not change appreciably following the exposure, which further testifies to its thermochemical stability. Figure 7 presents an SEM micro-image of the surface morphology of TiCrAlYO coating after a 1500 h exposure to 800°C moisturized air. The surface shows no considerable difference with the typically columnar morphology of the as-deposited coating, giving additional indication of its thermal stability. The dome-like surface morphology is developed during LAFAD coating deposition process which can be explained by a thermodynamically driven tendency of reducing the total surface energy during formation of the coating. Intense ion bombardment during LAFAD coating deposition process as well as self-sputtering can be mechanisms to contribute to formation of this surface pattern. The large dome-like surface morphology was also reported in ultra-thick TiN and TiAlN multilayer coatings deposited by LAFAD process.[38] The grooves between neighboring

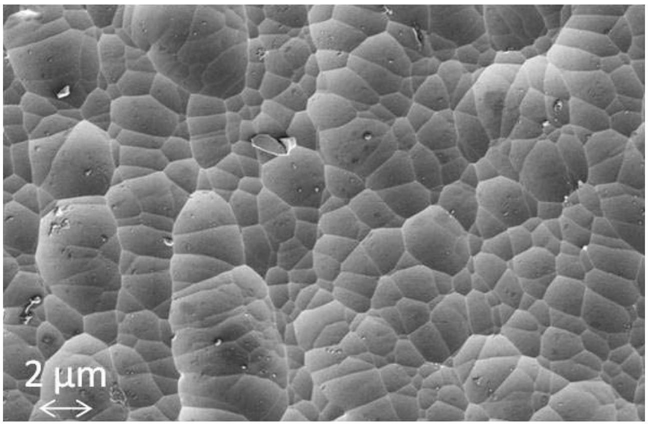

Figure 7. SEM micro-images of TiCrAlYO 12 μm thick LAFAD coating surface on SS substrate (Table II, Item 2) after 1500 h of exposure at 800°C in moisturized air.

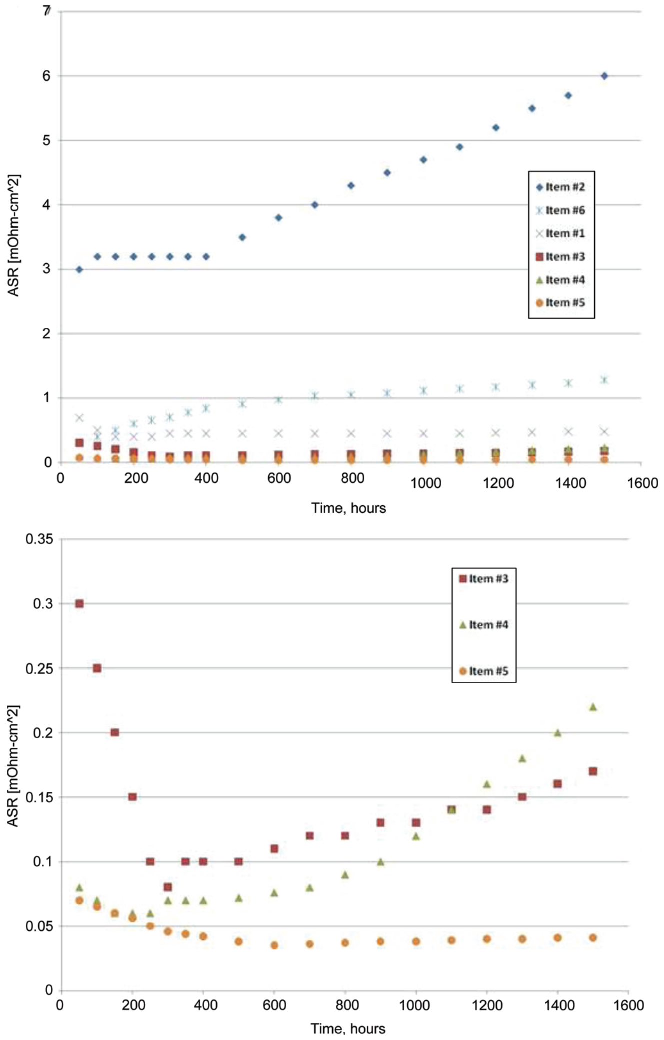

Figure 8. (Color online) ASR data for LAFAD coatings presented in Table II: higher scale (top); lower scale (bottom). LSM contact in 800°C air.

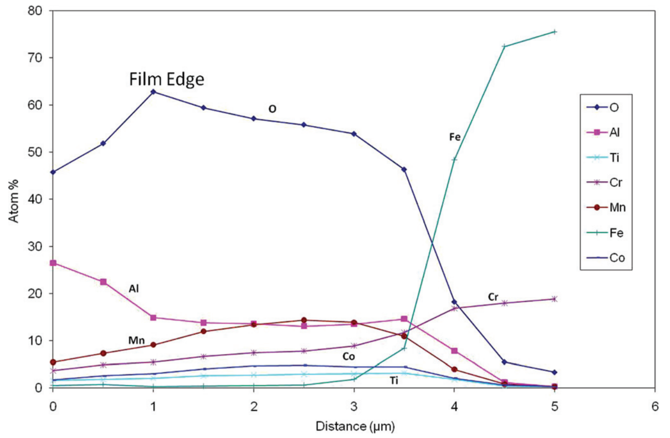

Figure 9. (Color online) EDS line scan across 3 μm thick CoMnTiCrAlYO coating as deposited (see sample ID in Table II, item 5).

domes are increasing during high temperature exposure: the grooves in TiCrAlYO coatings subjected to 1500 oxidation at 800°C are much deeper than that of as deposited coating. This can be attributed to thermal grooving phenomena. In this process, species transport takes place by surface diffusion along the interfaces, by volume diffusion through bulk or by evaporation–condensation mechanism resulting in a thermodynamically favorable reduction of the total surface energy.[39]

Figure 8 presents ASR data from the coatings described in Table II. The ASR values for all of these coatings having a thick TiCrAlYO bond interlayer (Table II, all items except the Item No. 5) are prohibitively high for the SOFC(IC) application. Figure 8 (bottom) presents ASR data from Fig. 8 (top), emphasizing the lowest ASR coatings. It has been demonstrated by this work that small variations in coating elemental composition result in substantial differences in ASR, thus ASR can be effectively engineered into SOFC(IC) coatings, if the coating deposition system permits elemental-level control, such as is the case for LAFAD coating system. The best ASR results were obtained on samples made of 441 SS with a CoMnTiCrAlYO coating (Table II, item 5) having a thickness of $\sim$3 μm and deposited with an ultra-thin TiCrAlYO bond layer (<50nm). The elemental composition of this coating is shown by the EDS line scan in Fig. 9. It can be seen from the ASR results presented in Fig. 8 that this coating has a low ASR (<50 mΩ· cm^2), which does not increase noticeably after 1500 h of high temperature exposure in contrast with all the other coatings. This nanocomposite multi-elemental oxi-ceramic coating can be considered as the most promising candidate for SOFC-IC application. Still, the optimal thickness and elemental composition of this coating has to be further optimized to meet performance requirement when deposited on actual IC plates. It has to be noted that an Al-rich bond interfacial sublayer, which is very useful to improve coating adhesion, is detrimental to ASR values. Therefore, the adhesion and cohesion toughness of the coating, as well as its high temperature thermal-mechanical stability and barrier properties vs their electronic conductivity have to be secured via adjustment of coating composition with the balance between AlCrO component responsible for the barrier properties and CoMnO components responsible for electronic conductivity, while keeping the AlCrO rich interfacial sublayer at lowest thickness range. The thickness of the coating must also be optimized. It can be noted that even with an AlCrO based oxiceramic coating as thin as 0.3 μm, a considerable reduction of TGO growth was obtained as presented elsewhere.[24] Figure 10 illustrates this case with SEM cross section images of a CoMnTiCrAlYO coating (Table II, item #5), which shows excellent adhesion and stability (minimal TGO growth) after up to 1500 h in 800°C air. While the coating is stable (minimal thickness changes), the coating elemental composition stratifies during the exposure, which helps explain the changing ASR values during IC and stack testing, as discussed below.

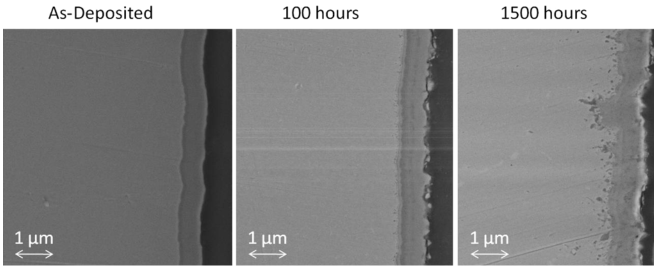

Figure 10. SEM cross-section of the optimized CoMnTiCrAlYO nanocomposite coating (Table II, Item #5) as-deposited and after high temperature exposure in ASR test environment.

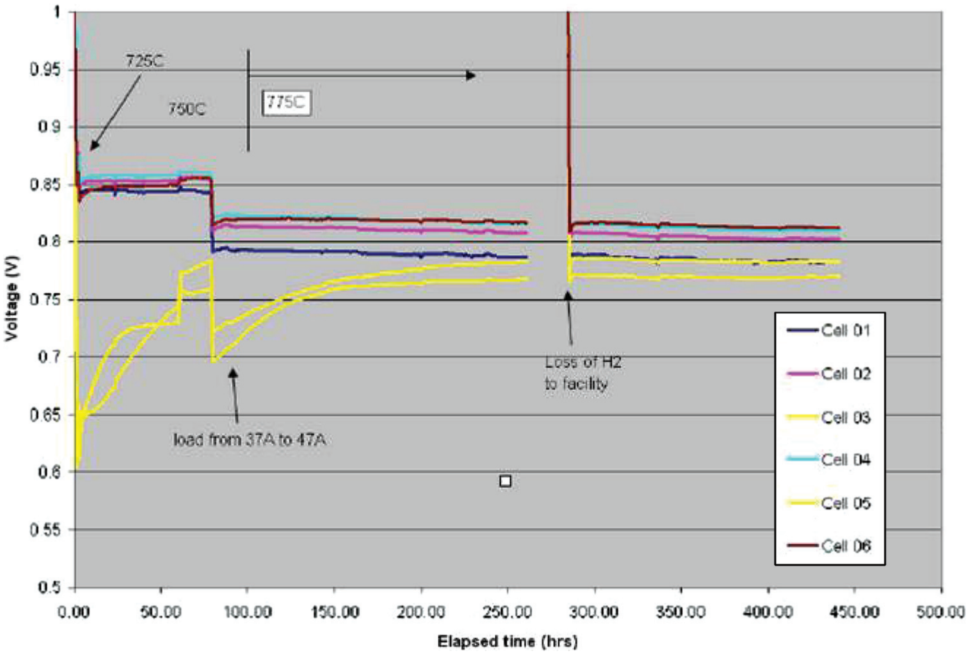

Figure 11. (Color online) Voltage drop across 6 test cells during 450 h test in SOFC stack at VPS. Cells #3 and #5 were provided with CoMnTiCrAlYO nanocomposite coating having ultra-thin alumina-rich adhesive bond layer as presented in Table II, item #5 (courtesy of Versa Power Systems).

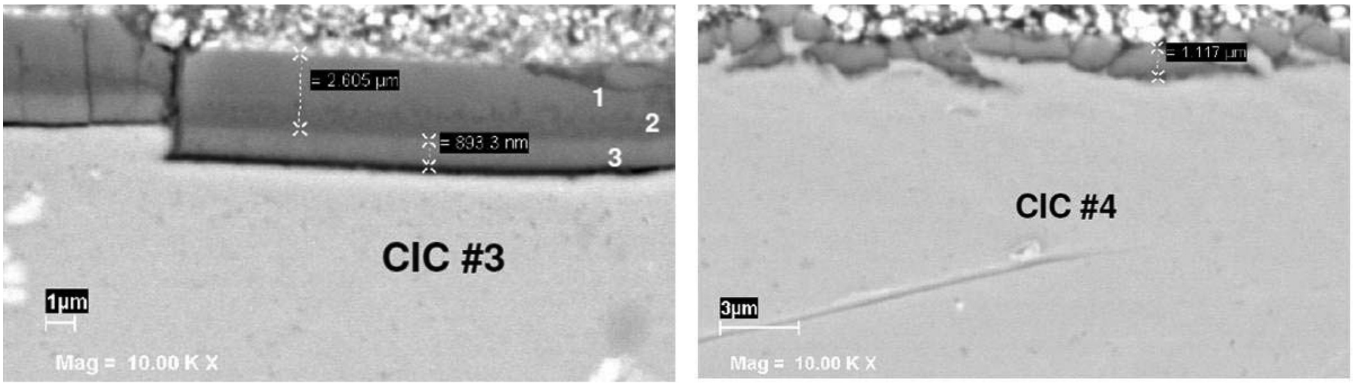

Spectrum	Al	Ti	Cr	Mn	Fe	Co	Y	O
1	13.99	1.52	8.33	16.37	0.59	6.02	0.29	52.89
2	14.76	2.84	10.75	12.00		5.46	0.41	53.79
3	6.91	1.02	22.79	10.89	2.88	5.17		50.33

Figure 12. SEM cross section of SOFC IC coupons with (top left) and without (top right) CoMnCTiCrAlYO nanocomposite coating with ultra-thin alumina-rich bond layer (Table II, item #5) and composition (bottom) of three distinct areas of the coating after 400 h testing in SOFC stack at 750°C (courtesy of Versa Power Systems)

Characterization of LAFAD protective coatings performance in a SOFC stack.— An optimized nanocomposite coating (Table II, item #5) deposited with an ultra-thin, Al-rich, bond layer (<4 nm) was tested within SOFC stacks by VPS to determine the efficacy of the coating strategy developed through this program. This optimized CoMnTiCrAlYO nanocomposite coating having an ultra-thin alumina-rich bond layer (Table II, item #5) was tested in a six-cell stack at VPS. The six-cell SOFC test stack included two coated interconnects in contact with cells #3 and #5 (CoMnTiCrAlYO coating (Table II, item #5)). The other three cells were connected with uncoated interconnects. The objective of this test was to study the effect of the protective coating on degradation and performance vs temperature and test duration time and to compare the results with a standard stack. Stack cell voltage profiles are presented in Fig. 11. Cells #3 and 5 initially showed low-voltages, but recovered significantly with time, reaching comparable levels with other cells by the end of the 450 h test. These coatings performed significantly better than those with thicker alumina-rich bond layers (e.g., coating #4 in Table II).

SEM images of the cross-sections of the coated and uncoated coupons taken from the interconnects subjected to this test are shown in Fig. 12, which reveals a substantially inhibited TGO growth on the coated interconnect. Although the optimized oxi-ceramic coating of Table II, item #5, underwent the entire 450 h SOFC stack test, the performance of the IC's with this coating was still lower than that of the uncoated samples due to the high electrical resistivity of this coating. This coating has demonstrated exceptionally good adhesion and protective properties; the voltages improved during a hold at high temperature but were still lower than those of other cells. The cross section of these coated interconnects in a post-test analysis revealed a high Al content of around 13 atom %. This amount is much lower than the previous tested interconnect coatings, which had 23 atom % of Al (Table II, item #4). Since the influence of the low-conductivity bond layer on the overall electrical conductivity of this coating has been eliminated, the next step toward optimization of this coating for SOFC-IC applications will be to further reduce the non-conductive, alumina-rich phases in this nanocomposite coating.

Summary

The continued TGO scale growth observed on uncoated FSS coupons makes them unsuitable for long-term use as SOFC interconnects. For this reason, it is imperative to develop effective protective coatings. An advanced coating deposition process has been developed to enable the use of inexpensive metallic alloys as interconnect components in planar SOFC systems. Significant improvements over uncoated SS was observed by the use of LAFAD coatings:

- Lower and more stable ASR values;
- Improved high-temperature oxidation resistance; and,
- Nearly complete inhibition of Cr volatility.

Exceptional high temperature stability was demonstrated by a nanocomposite TiCrAlYO coating deposited by the unidirectional LAFAD vapor plasma source. This coating retains its chemical, structural and mechanical properties, with excellent adhesion after 1500 h at 800°C in the ASR test environment. However, since this coating is a poor conductor, it cannot be used as a protective coating for the FSS ICs without the addition of other elements. This coating can be recommended for a seal of the SOFC-ICs. The addition of Co and Mn to the basic TiCrAlYO composition has demonstrated good potential by forming electronically conductive spinel phases, which are thermochemically stable and can survive long-term exposures in the SOFC-IC environment. Preliminary testing of the prototype metal ICs with LAFAD coatings in a SOFC stack has demonstrated that optimizing the CoMnO content in the TiCrAlYO matrix, while keeping the TiCrAlYO bond layer within an ultra-thin range can provide high electrical conductivity, excellent thermal-mechanical stability, and good diffusion-barrier properties for the coated ICs during long term service life in thermal cyclic conditions. More work is needed to optimize this promising coating composition and structure, with the optimal thickness expected to be in the range between 0.5–3 µm. The high deposition rate of this coating by the LAFAD process which surpasses other conventional vacuum processing technologies makes it a cost effective approach in mass production of SOFC components

Acknowledgments

We acknowledge the technical assistance of T. Wittberg, P. White, and W. Priyantha for sample preparation and various surface analyses. Thanks are also due to L. Pederson, J. Stevenson and

Z.G. Yang for fruitful discussions and for the exchange of the results of evaluation of different coatings for SOFC IC applications. Special thanks to Versa Power Systems for stack testing. Portions of this research were supported by the DOE under contract DE-FC26-04NT42225. Work at MSU was supported through the High-temperature Electrochemisty Center (HiTEC) DOE subcontract from PNNL, number 3917(413060-A). Finally, we acknowledge the helpful direction and support by DOE program managers, T. Schultz, A. Manivanan and B. White.

References

1. S. C. Singhal and K. Kendall, *High-Temperature Solid Oxide Fuel Cells: Fundamentals, Design and Applications*, Elsevier Science, Oxford (2004).
2. P. E. Gannon, C. T. Tripp, A. K. Knospe, C. V. Ramana, M. Deibert, R. J. Smith, V. I. Gorokhovsky, V. Shutthanandan, and D. Gelles, *Surf. Coat. Technol.*, **188–189**, 55 (2004).
3. M. Williams, in *Proceedings of the 7th International Symposium on Solid Oxide Fuel Cells*, S. C. Singhal and H. Yokakawa, editors, pp. 3–7, The Electrochemical Society, Inc., Pennington, NJ (2003).
4. Z. Yang, K. S. Weil, D. M. Paxton, and J. W. Stevenson, *J. Electrochem. Soc.*, **150**, A1188 (2003).
5. Crofer 22 APU "High Temperature Alloy" MSDS No. 8005 June, 2004 Thyssen-Krupp VDM.
6. Z. Yang, J. S. Hardy, M. Walker, G. Xia, S. P. Simner, and J. W. Stevenson, *J. Electrochem. Soc.*, **151**, A1825 (2004).
7. V. Gorokhovsky, "LAFAD-Assisted Plasma Surface Engineering Processes for Wear and Corrosion Protection: A Review," In Advanced Ceramic Coatings and Interfaces V: Ceramic Engineering and Science Proceedings Vol. **31**, No. 3, Ed. by Dongming Zhu, Hua-Tay Lin, 204 pg. Sponsoring by American Ceramic Society.
8. K. Hilpert, D. Das, M. Miller, D. H. Peck, and R. Wei, *J. Electrochem. Soc.*, **143**, A1896 (1996).
9. S. Elangovan, S. Balagopal, M. Timper, I. Bay, D. Larsen, and J. Hartvigsen, *J. Mater. Eng. Perform.*, **13**, 265 (2004).
10. Y. Yoo and M. Dauga, in *Proceedings of the 7th International Symposium on Solid Oxide Fuel Cells*, S. C. Singhal and H. Yokakawa, Editors, pp. 837–846, The Electrochemical Society, Inc., Pennington, NJ (2001).
11. N. Oishi, T. Namikawa, and Y. Yamazaki, *Surf. Coat. Tech.*, **132**, 58 (2000).
12. M. Kawate, A. K. Hashimoto, and T. Suzuki, *Surf. Coat. Technol.*, **165**, 163 (2003).
13. O. Banakh, P. E. Schmid, R. Sanjines, and F. Levy, *Surf. Coat. Technol.*, **163**, 57 (2003).
14. S. PalDey and S. C. Deevi, *Mater. Sci. Eng.*, **A342**, 1/2, 58 (2003).
15. Z. Yang, G. Xia, S. P. Simmer, and J. Stevenson, *J. Electrochem. Soc.*, **152**, A1896 (2005).
16. L. R. Pederson, P. Singh, and X.-D. Zhou, *Vacuum*, **80**, 1066 (2006).
17. P. Huczkowski, N. Christicmsen, V. Shemet, L. Niewolak, J. Piron-Abellan, L. Singheiser, and W. J. Quadakkers, *Fuel Cells*, **6**, 93 (2006).
18. M. Stanislowski, J. Froitzheim, L. Niewolak, W. J. Quadakkers, K. Hilpert, T. Markus, and L. Singheiser, *J. Power Sources*, **164**, 578 (2007).
19. R. L. Boxman, D. M. Sanders, and P. J. Martin, *Handbook of Vacuum Arc Science and Technology*, Noyes Publications, Park Ridge, NJ (1995).
20. R. Wei, E. Langa, C. Rincon, and J. H. Arps, *Surf. Coat. Technol.*, **201**, 4453 (2006).
21. J. Musil, in *Nanostructured Coatings*, A. Cavaliero and J. De Hosson, Editors, Springer, New York (2006).
22. V. I. Gorokhovsky, R. Bhattacharya, and D. G. Bhat, *Surf. Coat. Technol.*, 2001, **140**, 82 (2001).
23. V. Gorokhovsky, C. Bowman, D. VanVorous, and J. Wallace, *J. Vac. Sci. Technol. A*, **27**, 1080 (2009).
24. V. I. Gorokhovsky, P. E. Gannon, M. C. Deibert, R. J. Smith, A. Kayani, M. Kopczyk, D. VanVorous, Z. Yang, J. W. Stevenson, S. Visco et al., *J. Electrochem. Soc.*, **153**, A1886 (2006).
25. V. Gorokovsky, C. Bowman, P. E. Gannon, D. VanVorous, J. Hu, C. Muratore, A. A. Voevodin and Y. S. Kang, *Wear*, **265**, 741 (2008).
26. R. J. Smith, C. Tripp, A. Knospe, C. V. Ramana, A. Kayani, V. Gorokhovsky, V. Shutthanandan, and D. S. Gelles, *J. Mater. Eng. Perform.*, **13**, 295 (2003).
27. J. Suchet and N'Guen Thien-Chi, U.S. Pat. 2,720,471 (1955).
28. H. Jehn, G. Reiners, N. Siegel, DIN-Fachbericht (Special Report) 39, Charakterisierung duenner Schichten (Characterization of thin layers), Beuth-Verlag, Berlin, 1993.
29. M. Mayer, SIMNRA User's Guide, Technical Report IPP 9/113, Max-Planck-Institut fur Plasmaphysik, Garching, Germany (1997).
30. J. R. Tesmer and M. Nastasi, *Handbook of Modern Ion Beam Materials Analysis, Materials Research Society*, Pittsburgh, PA (1995).
31. C. Collins, J. Lucas, T. L. Buchanan, M. Kopczyk, A. Kayani, P. E. Gannon, and V. I. Gorokhovsky, *Surf. Coat. Technol.*, **201**, 446 (2006).
32. H. Chen, J. A. Lucas, W. Priyantha, M. Kopczyk, R. J. Smith, K. Lund, C. Key, M. Finsterbusch, P. E. Gannon, and M. Deibert et al., *Surf. Coat. Technol.*, **202**, 4830 (2008).
33. N. A. Vatolin, G. K. Moiseev, and B. G. Trusov, *Thermodynamic Modeling in High Temperature Inorganic Systems*, Moscow, Metallurgy, 1994 (in Russian).
34. L. V. Gurvich, I. V. Veyts, and C. B. Alcock, *Thermodynamic Properties of Individual Substances*, 4th edition in 5 Volumes, Vol. 1 in 2 parts, Hemisphere Pub. Co., New York, London (1989).
35. *NIST-JANAF Thermochemical Tables*, 4th ed., M. W. Chase, Jr., Editor, Journal of Physical and Chemical Reference Data, Monogr. 9 (1998).
36. V. Gorokhovsky, C. Bowman, P. Gannon, D. Van Vorous, A. Voevodin, A. Rutkowski, C. Muratore, R. J. Smith, A. Kayani, D. Gelles, et al., *Surf. Coat. Technol.*, **201**, 3732 (2006).
37. A. Kayani, R. J. Smith, S. Teintze, M. Kopczyk, P. E. Gannon, M. C. Deibert, V. I. Gorokhovsky, and V. Shutthanandan, *Surf. Coat. Technol.*, **201**, 1685 (2006).
38. V. I. Gorokhovsky, *Surf. Coat. Technol.*, **204**, 1216 (2010).
39. S. Bhowmick, J. L. Riesterer, Y. Xue, and C. Barry Carter, in *Advances in Solid Oxide Fuel Cells V*, N. P. Bansal, P. Singh, D. Singh, and J. Salem, Editors, Wiley, Hoboken, NJ USA (2010).